Molecular hydrogen absorption systems in Sloan Digital Sky Survey

S. A. Balashev, V. V. Klimenko, A. V. Ivanchik, D. A. Varshalovich, P. Petitjean, P. Noterdaeme

HAL Id: insu-03645657
https://insu.hal.science/insu-03645657

Submitted on 25 Apr 2022

Molecular hydrogen absorption systems in Sloan Digital Sky Survey

S. A. Balashev,[1,2]★ V. V. Klimenko,[1,2] A. V. Ivanchik,[1,2] D. A. Varshalovich,[1,2]
P. Petitjean[3] and P. Noterdaeme[3]

[1]*Ioffe Physical-Technical Institute of RAS, Polyteknicheskaya 26, 194021 Saint-Petersburg, Russia*
[2]*St.-Petersburg State Polytechnical University, Polyteknicheskaya 29, 195251 Saint-Petersburg, Russia*
[3]*Institut d' Astrophysique de Paris, UPMC-CNRS, UMR7095, 98 bis boulevard Arago, F-75014 Paris, France*

ABSTRACT

We present a systematic search for molecular hydrogen absorption systems at high redshift in quasar spectra from the Sloan Digital Sky Survey (SDSS)-II Data Release 7 and SDSS-III Data Release 9. We have selected candidates using a modified profile fitting technique taking into account that the Lyα forest can effectively mimic H$_2$ absorption systems at the resolution of SDSS data. To estimate the confidence level of the detections, we use two methods: a Monte Carlo sampling and an analysis of control samples. The analysis of control samples allows us to define regions of the spectral quality parameter space where H$_2$ absorption systems can be confidently identified. We find that H$_2$ absorption systems with column densities log $N_{H_2} > 19$ can be detected in only less than 3 per cent of SDSS quasar spectra. We estimate the upper limit on the detection rate of saturated H$_2$ absorption systems (log $N_{H_2} > 19$) in damped Lyα (DLA) systems to be about 7 per cent. We provide a sample of 23 confident H$_2$ absorption system candidates that would be interesting to follow up with high-resolution spectrographs. There is a 1σ $r - i$ colour excess and non-significant A_V extinction excess in quasar spectra with an H$_2$ candidate compared to standard DLA-bearing quasar spectra. The equivalent widths of C II, Si II and Al III (but not Fe II) absorptions associated with H$_2$ candidate DLAs are larger compared to standard DLAs. This is probably related to a larger spread in velocity of the absorption lines in the H$_2$-bearing sample.

Key words: ISM: clouds – quasars: absorption lines – cosmology: observations.

1 INTRODUCTION

The Sloan Digital Sky Survey (SDSS; York et al. 2000) is one of the largest optical surveys of modern astrophysics. One of the major goals of this survey is to study large-scale structures in the nearby Universe $z < 0.7$, from the spatial distribution of galaxies (York et al. 2000). The survey targets millions of objects (galaxies, stars and quasars) by imaging and spectroscopy in the optical wavelength band. The recently published Data Release 9 (DR9; Ahn et al. 2012) contains over 80 000 spectra of high-redshift quasars (Pâris et al. 2012).

Absorption lines in quasar spectra allow one to study the intergalactic and interstellar matter located along the line of sight to the quasar. Quasars are routinely detected up to $z \sim 6$, which corresponds to more than 12 Gyr ago. The Baryon Oscillation Spectroscopic Survey (BOSS; Schlegel et al. 2007; Dawson et al. 2013), one of the main projects of SDSS-III (the third generation of SDSS), is primarily focused on the analysis of the spatial distribution of

luminous red galaxies (LRGs) and absorptions in the Lyα forest. The later enables to determine the baryon acoustic oscillation (BAO) scale at $z \sim 2.5$ that corresponds to an epoch before dark energy dominates the expansion of the Universe (Busca et al. 2013). In addition to this primary goal, BOSS spectra will allow one to study of broad absorption line (BAL) systems arising in the vicinity of active galactic nucleus (AGN), as well as intervening metal absorption line systems (such as C IV and Mg II) associated with clouds located into the halo of intervening galaxies (Quider et al. 2011; Zhu & Ménard 2013).

Damped Lyα systems (DLAs) are identified by a broad H I Lyα absorption line with prominent saturated Lorentz wings. Statistical analysis shows that DLAs are the main reservoir of neutral gas at high redshifts (Noterdaeme et al. 2009; Prochaska & Wolfe 2009). It is believed that these systems are associated with discs of galaxies or their close vicinity with impact parameter less than 20 kpc (Fynbo et al. 2011; Krogager et al. 2012). Numerous species are seen in DLAs (e.g. C I to C IV and Si I to Si IV) and the typical velocity spread of metal absorption lines is about 100–500 km s^{-1}. All this makes DLAs relatively easy to detect at intermediate resolution. About 12 000 DLA/sub-DLA candidates with log N(H I) ≥ 20 were

detected in SDSS-DR9 (Noterdaeme et al. 2012). It has been shown that a small fraction of DLAs host molecular hydrogen (Noterdaeme et al. 2008a) which corresponds to diffuse and translucent neutral clouds embedded in warm neutral interstellar medium (ISM). In some cases HD molecules are detected (Varshalovich et al. 2001; Noterdaeme et al. 2008b; Balashev, Ivanchik & Varshalovich 2010) as well as CO molecules (Srianand et al. 2008; Noterdaeme et al. 2011). Observations of molecular hydrogen clouds at the high-redshift Universe provide a unique opportunity to study several issues. Molecular hydrogen is believed to be an indicator of the cold phase of the ISM which is the raw material for the star formation – it was found that regions with high H_2 abundance are correlated with the star formation regions (Krumholz 2012). The measurement of relative abundances of different H_2 rotational levels allows one to determine the physical conditions in this cold ISM – kinetic temperature, ultraviolet (UV) radiation field and possibly number density. There are several cosmological problems related to high-redshift molecular hydrogen absorption systems: (i) the detection of HD gives the possibility of a complementary approach to the determination of the primordial deuterium abundance (Balashev et al. 2010; Ivanchik et al. 2010); (ii) constraints on the possible variation of the proton to electron mass ratio can be obtained (e.g. Thompson 1975; Ivanchik et al. 2005; Wendt & Molaro 2012; Rahmani et al. 2013); (iii) the cosmic microwave background radiation (CMBR) temperature can be measured at high redshift from the populations of the CO rotational levels (e.g. Noterdaeme et al. 2011) and C I fine-structure levels (e.g. Songaila et al. 1994; Srianand, Petitjean & Ledoux 2000).

Since the first detection by Levshakov & Varshalovich (1985), about 20 H_2 absorption systems have been detected at high redshifts ($z > 1$; see Ge & Bechtold 1997; Ledoux, Srianand & Petitjean 2002; Ledoux, Petitjean & Srianand 2003; Reimers et al. 2003; Cui et al. 2005; Noterdaeme et al. 2008a, 2010; Srianand et al. 2008; Jorgenson et al. 2009; Jorgenson, Wolfe & Prochaska 2010; Malec et al. 2010; Fynbo et al. 2011; Guimarães et al. 2012). Additionally, two systems were detected in spectra of gamma-ray burst (GRB) afterglows (Prochaska et al. 2009; Krühler et al. 2013), one system was detected at intermediate redshift $z \sim 0.5$ (Crighton et al. 2013) and four systems (Noterdaeme et al. 2009, 2011) were detected by means of CO molecules (H_2 and HD transitions in these systems are redshifted out of the observed wavelength range). Most of the detection of molecular hydrogen absorption systems have been performed with high signal-to-noise ratio (S/N) and high-resolution spectra with typically 3 h exposures on an 8-m class telescope. On the other hand, there are about 80 000 high-redshift quasar spectra obtained in the course of SDSS to be search for H_2. The main disadvantages of SDSS spectra for detection of molecular hydrogen systems are that they have intermediate spectral resolution $R \sim 2000$ and usually low S/N (<4 over the wavelength range where H_2 absorption lines are to be found).

In this paper we show however that it is possible to find H_2-bearing systems in SDSS spectra provided that the column density is large enough. Although such systems are rare, the large number of SDSS quasar spectra makes their detection possible. We provide a list of H_2 candidates for follow-up with high-resolution observations. The paper is organized as follows. In Section 2 we give a brief description of the data. Section 3 describes a searching criterion to be used. We define a quantitative estimate of the confidence level or false identification probability (FIP) in Section 4. The final list of the H_2 system candidates is given in Section 5 and we investigate some properties of this sample in Section 6 before conclusions are drawn in Section 7.

2 DATA

We used the spectroscopic data from the SDSS. The DR9 (Ahn et al. 2012) presents the first spectroscopic data from the BOSS (Schlegel et al. 2007; Dawson et al. 2013) and contains 87 822 primarily high-redshifted quasars (78 086 are new detections) detected over an area of 3275 deg². The data from previous parts of projects SDSS-I and SDSS-II were presented in the Data Release 7 (DR7; Abazajian et al. 2009) and quasar catalogues (Schneider et al. 2010) include 105 783 quasars in an area of 9380 deg². Since SDSS-III preferentially targets high-redshift quasars, most of the searched spectra are from DR9. In addition, we found that the improved quality of the BOSS spectra is an important factor for the detection of H_2 absorption systems. However, we also applied our searching routine to the DR7 catalogue. The spectrum of J153134.59+280954.36 is shown in Fig. 1 as an example.

It is commonly accepted that H_2 molecular clouds are related to the neutral medium. Hence high column density ($\log N > 16$, N in cm^{-2}) H_2 absorption systems have to be associated with large amount of neutral hydrogen, i.e. to be associated with DLAs. Since the Lyα transition being at 1215.67 Å, DLAs in SDSS can be identified only for redshifts $z \gtrsim 2.15$ and $\gtrsim 2$ for DR7 and DR9, respectively. This gives 14 616 quasar spectra from SDSS-DR7 and 61 931 from BOSS SDSS-DR9. In these spectra 1426 and 12 068 DLAs were detected in DR7 (Noterdaeme et al. 2009) and DR9 (Noterdaeme et al. 2012), respectively. Note that a part of high-redshift DR7 spectra was re-observed by BOSS therefore some fraction of quasars is common to both DR7 and DR9.

We used only quasar spectra for which at least one H_2 absorption line associated with corresponding DLA system falls in the SDSS wavelength range. The blue limits of the SDSS-II and BOSS spectrographs are 3800 and about 3570 Å, respectively. Molecular hydrogen lines from J = 0, 1 levels are located in the wavelength range 912–1110 Å in rest frame (see Fig. 1). It restricts redshifts of suitable DLAs to values $z_{DLA} > 2.42$ and >2.22 from DR7 and DR9, respectively. About 1200 and 10 000 quasar spectra satisfy this criteria from DR7 and DR9, respectively. These quasars make up the sample (which we refer below as S_{DLA}) to search for H_2 absorption systems.

We additionally have built the sample of non-BAL and non-DLA quasar spectra from SDSS DR9 catalogue which satisfied our quasi-stellar object (QSO) redshift and S/N conditions ($z_{QSO} > 2.22$ and $S/N > 2$). We denote this sample as S_{nonDLA}. It contains about 40 000 quasar spectra. In principle, we can expect that spectra from this sample contain no or very few[1] H_2 absorption systems because no corresponding DLAs were found. This sample will be used as a control sample to test the searching routine and to estimate the detection limit of H_2 absorption systems.

3 SEARCH OF H₂ ABSORPTION SYSTEMS

With such a large number of spectra we need an automatic procedure to search for H_2. For this purpose we used a modification of the standard profile fitting technique which compares an observed quasar spectrum with a synthetic H_2 absorption spectrum.

---

[1] Although the completeness of the DLA sample is not unity, in particular at the low N(H I) end, the overwhelming number of spectra will not contain H_2 system.
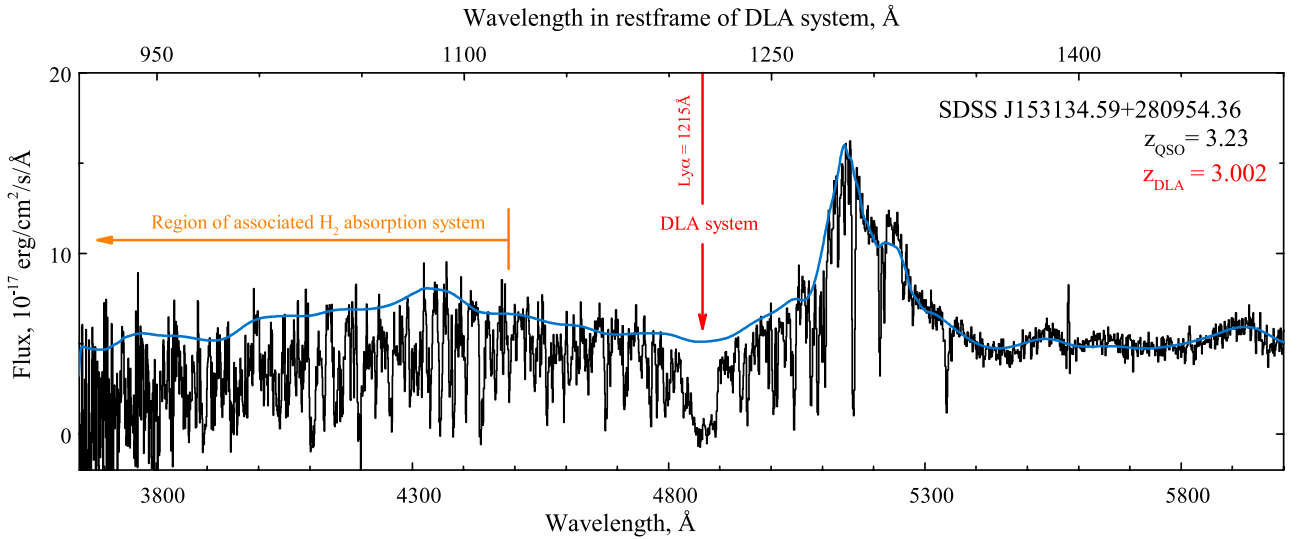
Figure 1. SDSS spectrum of quasar J153134.59+280954.36 ($z_{QSO} = 3.23$). The top axis shows the wavelength scale in the rest frame of the DLA system which was identified at $z_{DLA} = 3.002$. The orange line marks the region of the spectrum where H₂ absorptions (associated with the DLA system) are located. Note that the S/N ratio in this region is about 10, which is well above the median S/N of the SDSS spectra. The blue curve shows the estimated quasar unabsorbed continuum.

3.1 Continuum determination

The determination of the quasar continuum is the first important step of any profile fitting routine. We used a combination of two methods: the principal component analysis (PCA) and the iterative smoothing.

The first method reproduces an unabsorbed flux over the Lyα forest by fitting the red part of the spectrum with a combination of principal components (see Pâris et al. 2011). We need to define the continuum in a wider wavelength range ($900 < \lambda < 1200$ Å in the rest frame of the quasar) compared to what was done by Pâris et al. (2011), they reconstructed continuum between the Lyβ and C IV emission lines. To expand the continuum to the region $\lambda < 1025$ Å we used a power-law extrapolation of the mean quasar continuum (used in PCA method) adding features which account for the Lyβ emission line and the Lyman break cut-off.

In the second method the spectrum is smoothed iteratively. For each iteration we smoothed the spectrum by convolution with a Gaussian function with full width at half-maximum (FWHM) about 50 Å. Then pixels deviating from the continuum by more than 3σ are excluded at each iteration. The remaining pixels were used in the next iteration. We used four iterations, which was enough for convergence.

We found that the first method tends to overestimate the continuum and sometimes yields an incorrect shape in the presence of sharp features, while the second method tends to underestimate the continuum and to smooth out emission lines. Therefore, the final continuum was constructed as the geometric average of the two continua convolved with a Gaussian function with FWHM ~ 1000 km s^{-1} (an example of reconstructed continuum is shown in Fig. 1). Obviously, the continuum reconstruction in the region bluewards the Lyα emission line is rather difficult and sometimes ambiguous. Nevertheless, simulations presented in Section 3.3 show that the continuum reconstructed by the described procedure does not introduce any strong bias in the search for H₂ absorption systems. For each spectrum in the samples we determined the S/N as the mean of S/N in each pixel over the wavelength range 1120–1040 Å in the rest frame of the DLA system.

3.2 The searching procedure

Three main difficulties complicate the identification of H₂ absorption systems in SDSS spectra: (i) the intermediate spectral resolution; (ii) the usually low S/N and (iii) the presence of the Lyα forest. These difficulties jointly can lead to false identifications of H₂ absorption systems. The SDSS spectral resolution is the most important of them. The pixel size in the blue part of the SDSS spectrum is about 1 Å. It sets a lower limit on the equivalent width (EW) of the H₂ lines which can be identified in SDSS spectra. The condition that H₂ EWs to be larger than 1 Å is fulfilled only for H₂ column density larger than $\log N_{H_2} \gtrsim 18.5$. The molecular hydrogen absorption spectrum in the UV appears as a series of absorption lines corresponding to Lyman and Werner vibrational bands Lν-0 and Wν-0. Intermediate SDSS spectral resolution leaves the possibility to observe only the most prominent lines corresponding to the R(0), R(1) and P(1) transitions in each band. These three absorption lines for each band are overlapped with each other under such resolution. We will refer to these absorption features by the name of the band, i.e. in case L4-0R(0), L4-0R(1) and L4-0P(1) are overlapped, the absorption feature will be denoted as L4-0 absorption line. The typical shapes of these lines are shown in Fig. 2 by blue colour.

We will construct a template of H₂ absorption systems to fit the SDSS spectra. The H₂ absorption lines (from low rotational levels) have rest-frame wavelengths $\lambda < 1115$ Å. In principle, before the Lyman cut-off (at 912 Å) of the DLA system, 26 absorption lines (from the Lyman and Werner bands) can be observed. However, H I absorption lines of high-order Lyman series of the DLA system can substantially absorb the spectrum blueward of ~ 950 Å. At the SDSS resolution, it leaves only about 17 H₂ lines which can be identified in the spectrum. However, the number accessible H₂ absorption lines varies for different spectra primarily because of the difference between the DLA and quasar redshifts and also because of the spectrum quality (in SDSS spectra S/N usually decreasing with decreasing wavelength). If the quasar redshift is low, the blue end of the spectrum limits the number of fitted H₂ lines. If the quasar redshift is high ($z > 2.8$), then the presence of Lyman limit systems or saturated Lyα forest lines at redshift between z_{QSO} and z_{DLA} can
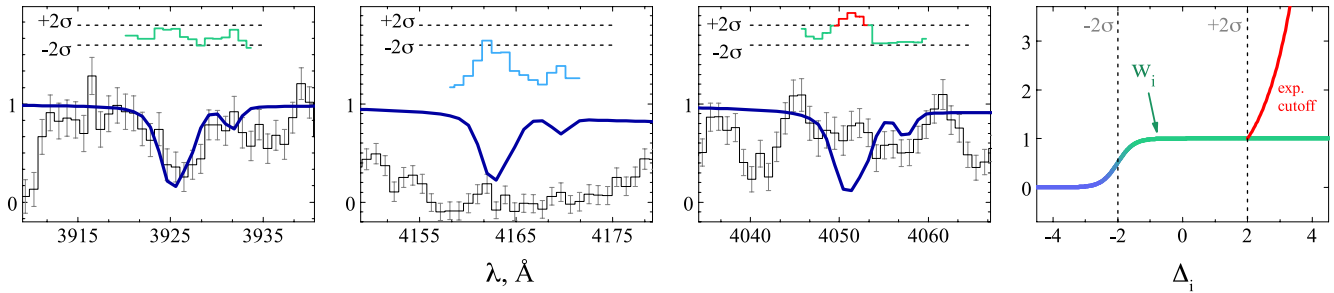
Figure 2. Illustration of the searching criterion. The three left-hand panels show different situations: respectively from left to right, good fit, blended and bad fit. The blue line shows typical profiles of highly saturated (e.g. $\log N_{H_2} = 20$) R(0), R(1) and P(1) lines convolved with the SDSS instrument function. The right-hand panel shows the weight function and exponential cut-off function that we used in our searching procedure (see equations 1 and 3).

reduce the number of H_2 lines in the fit. To characterize the number of fitted lines we determined the cut-off wavelength $\lambda_{\text{cut-off}}$ as the position in the spectrum from which the flux exceeds the zero level at the 2σ level over more than 4 pixels in a row. In the following we will use the parameter $\lambda_B = \lambda_{\text{cut-off}}/(1 + z_{\text{DLA}})$ – the cut-off in the spectrum expressed in the DLA rest frame. This parameter just characterizes the number of H_2 absorption lines, that was used in the fit. The pixels corresponding to the DLA Lyman series lines (Lyβ, Lyγ, etc.) were excluded from the fit.

To identify H_2 absorption systems we used the profile fitting technique which compares a real spectrum with an H_2 model spectrum with specified physical parameters (i.e. column density, Doppler parameter, redshift). As we have to search H_2 systems in the large number of spectra ($\sim$13 000), we need to develop an automatic procedure. We constructed a function based on the standard χ^2 likelihood function commonly used in profile fitting procedures. This function is defined as

$$\log L = \frac{\sum_i w_i \xi_i}{\sum_i w_i}, \tag{1}$$

where we introduced the weight w_i for each pixel:

$$w_i(\Delta_i) = \frac{1}{1 + e^{-4(\Delta_i + 2)}}, \tag{2}$$

where $\Delta_i = (y_i - f(x_i))/\sigma_i$ is the relative deviation of the model f_i from the observed flux y_i in pixel x_i, σ_i is the error in pixel x_i. The weight function w_i was chosen in the following way (see right-hand panel of Fig. 2). We rejected those pixels (i.e. their $w_i = 0$) for which the spectrum is more than 2σ below the model because they are possibly related to blends which are numerous in the Lyα forest. For pixels where $2 > \Delta_i > -2$, $w_i \approx 1$. The function ξ_i is given by

$$\xi_i = \begin{cases} \Delta_i^2 e^{(1-\Delta_i)^2 - 1}, & \Delta_i \geq 2, \\ \Delta_i^2, & \Delta_i < 2, \end{cases} \tag{3}$$

where for $\Delta_i \geq 2$, an exponential cut-off is introduced because in case H_2 is present, all the absorption lines should be consistently seen. Obviously, it is reasonable to fit only the absorbed part of the spectrum. Therefore the sum is taken only over the pixels where the model f is less than 0.9 times the continuum level. Note that the introduction of the exponential factors implies that L defined by equation (1) is not a likelihood function. The function L is used only to select H_2 system candidates. We will estimate the confidence level of the detection in Section 4. We set the criterion of identification as $L < L_{\text{id}}$, where L_{id} is the value of L with $\Delta_i = 2$ for all pixels ($w_i \approx 1$ when $\Delta_i = 2$) at certain redshift. This criterion is fulfilled in the case of the satisfactory fit of spectrum by H_2 absorption system

model, i.e. there are no outliers in pixels, where observed flux is sufficiently larger than fit flux.

In standard profile fitting the best fit is obtained by minimization of a likelihood function over the parameter space. However, such a process requires to calculate a large number of absorption profiles which in our case would be particularly computational demanding. Rather we constructed a set of H_2 absorption system template spectra on a dense grid of total column density and effective excitation temperature. These two parameters mainly define the line profiles of saturated H_2 absorptions at a given spectral resolution. The total H_2 column density ranges from $\log N(H_2) = 18.5$ to 21 by step of 0.1 dex. With column densities less than 18.5 the absorption lines become weak and reliable identification of H_2 is impossible (see Section 4.2). The effective excitation temperature, T_{01}, specifies the relative populations of H_2 $J = 0$ and $J = 1$ levels. T_{01} was varied from 25 to 150 K corresponding to the typical observed range (Srianand et al. 2005). The Doppler parameter is not important since we considered only highly saturated absorption systems ($\log N > 18.5$). An important ingredient is the velocity structure of the absorption system, i.e. the number of components, their relative strengths and positions. High-resolution observations show that more than 50 per cent of the H_2 absorption systems are multicomponent. However, the typical velocity separation of these components is less than 50 km s^{-1} which is smaller than the SDSS spectral resolution ($\sim$150 km s^{-1}). Therefore, we use a single-component model. This implies however that our inferred H_2 column densities can be overestimated. This is partially confirmed by the analysis of the H_2 systems previously identified in high-resolution spectra (see Section 5).

We have implemented a fully automatic searching procedure. For each spectrum in the S_{DLA} sample we calculated L function in the redshift window for each model of H_2 absorption system in the template. The redshift window was taken as ± 600 km s^{-1} around the redshift of the DLA system. The DLA redshifts were taken from Noterdaeme et al. (2009, 2012). Note that the value 600 km s^{-1} is larger than the typical observed velocity dispersion for H_2 absorption systems in DLAs. For each H_2 absorption system model from the template we have searched for redshifts at which identification criterion $L < L_{\text{id}}$ is satisfied. Note that function L guarantees that if H_2 absorption system with column density N_0 is satisfied $L < L_{\text{id}}$ for some position z then H_2 absorption system with column density $N < N_0$ (less saturated) will also satisfied $L < L_{\text{id}}$ at z.

Applying our searching procedure to the S_{DLA} sample we have selected a preliminary S_{cand} sample of H_2 system candidates. For each candidate in the sample we have recorded the largest total column density for which $L < L_{\text{id}}$ is satisfied and the value of z_0 where L

has minimum for this largest total column density. The preliminary sample of candidates, S_{cand}, contains over 4000 records. However most of these candidates are false detections caused mainly by Lyα forest features in low S/N spectra. Indeed the observed occurrence rate of H_2 candidate in DLA based on the preliminary sample ($\sim 4000/13\,000 = 0.3$) is larger than the <0.1 estimated rate based on high-resolution data (Noterdaeme et al. 2008a). To select most promising candidates for follow-up spectroscopic studies we need to select only candidates with high confidence, i.e. the candidates with a low probability of false detection. Two methods to estimate the probability of false detection are described in Section 4.

3.3 Testing the searching procedure

We need to be convinced that the overwhelming majority of real H_2 absorption systems will be detected by the searching procedure. One of necessary conditions is that the known H_2 absorption systems should be detected by our procedure in SDSS data. There are only five such systems with SDSS data. They are listed in Table 2 and will be discussed in Section 5. Only three of these spectra are useful because of the proper spectral wavelength range. The searching procedure detects H_2 in all of them. This is fine but not enough to be convinced of the robustness of the searching procedure. Therefore we have tested the searching procedure on the data where we artificially added H_2 systems. For this we have used the S_{nonDLA} sample (where there are no DLAs, see Section 2) and artificially added DLAs with one H_2 component with a specified column density N at a given redshift. We used each spectrum several times varying the DLA redshift to increase statistics. With this procedure we are sure that we have the same situation of noise and redshift distribution as in our search sample.

After applying our searching procedure we find that the typical non-detection rate (i.e. the fraction of systems we miss) is less than 1 per cent. The dependence of the non-detection rate with the specified column density is shown in Fig. 3.

We conclude that our searching procedure gives a sample which is complete at the >99 per cent level for log $N(H_2) > 18$. However, as we will show in the following section at such column densities the false identifications dominate the candidate sample and the limit column density for reliable identification is log $N(H_2) > 19$. For

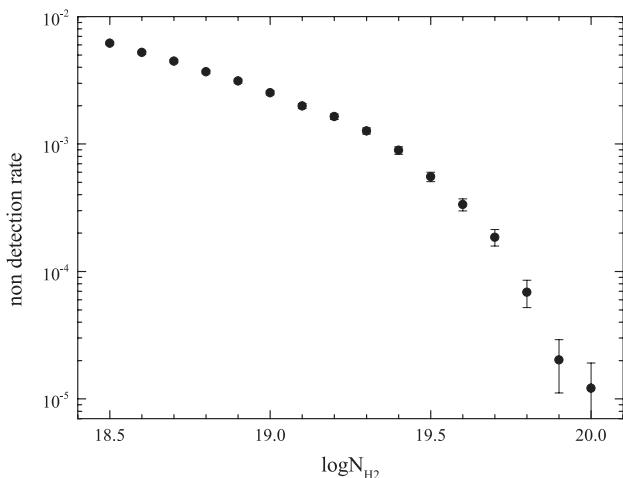**Figure 3.** Non-detection rate of the searching procedure versus log $N(H_2)$. This rate is found to be less than 1 per cent.

column density log $N(H_2) > 19$ our searching procedure gives completeness at more than 99 per cent level.

4 CONFIDENCE ESTIMATION

In the previous section we have shown that our procedure is able to identify strong H_2 absorption systems in SDSS spectra when they are present. However, at this resolution, the numerous Lyα forest lines can easily mimic an H_2 absorption system and lead to false identifications. Therefore, in order to select a robust sample of H_2 system candidates, we need to estimate the confidence level of the candidates, i.e. the probability for an H_2 candidate to be real. For this we determined a FIP. It is the probability to wrongly select an H_2 absorption system in some realization of the Lyα forest. If FIP is small, then the selected H_2 absorption system is likely to be real, i.e. its confidence value is high.

We have applied two methods for FIP determination. In the first method for each possible detection, we have calculated the probability that a similar absorption system is detected anywhere else in the spectrum (see Section 4.1). In the second method we have calculated the rate of H_2 absorption system identification in the samples of spectra where there are confidently no H_2 absorption systems, i.e. in control samples. The latter method presented in Section 4.2 allows us in addition to estimate a detection threshold of H_2 absorption system in SDSS spectra and the detection probability of H_2 absorption systems in DLAs.

4.1 Monte Carlo sampling

The main point of this method is H_2 absorptions to be numerous, so as a typical system will be detected by about 6–15 absorption features. Suppose that the probability to 'fit' by chance one H_2 line in the forest is 0.5. This means that the absorption line satisfies the identification criterion ($L < L_{id}$) over half of any wavelength window. Then the chance to 'fit' N lines together would be about $(0.5)^N$. The joint probability to fit an H_2 system by chance in a forest where no H_2 system is present can thus be very small. Therefore it is reasonable to expect that we can identify H_2 absorption systems even at the SDSS resolution and spectral quality.

To estimate the confidence of each candidate in the S_{cand} sample we used the following procedure. We performed arbitrary *random* shifts of the H_2 absorption lines detected in the candidate. The shift of each line was limited by the position of the adjacent H_2 lines in the spectrum, typically less than 4000 km s^{-1}. In other words, we randomly 'shake' the H_2 absorption line positions. We performed many realizations and for each one we calculated the value of the L criterion. The identification probability is estimated as

$$f_{FP} = n(L < L_{id})/n_{all},$$

where $n(L < L_{id})$ is the number of identifications, i.e. realizations that satisfied ($L < L_{id}$), and n_{all} is the total number of realizations. The value of f_{FP} can be simply described as the probability of joint fit of several absorption lines in the particular realization of the Lyα forest in the spectrum. If $L < L_{id}$ for the majority of realizations, then $n(L < L_{id})$ is close to n_{all} and f_{FP} is close to 1. In this case Lyα forest can effectively mimic the absorption system and the identification cannot be considered as robust. If $L < L_{id}$ in a few of many realizations, then f_{FP} approaches 0. In this case the probability of the Lyα forest to mimic the absorption system is small and the confidence in the identification of the system is high. It should be emphasize that this method takes naturally into account the peculiarities of each spectrum.
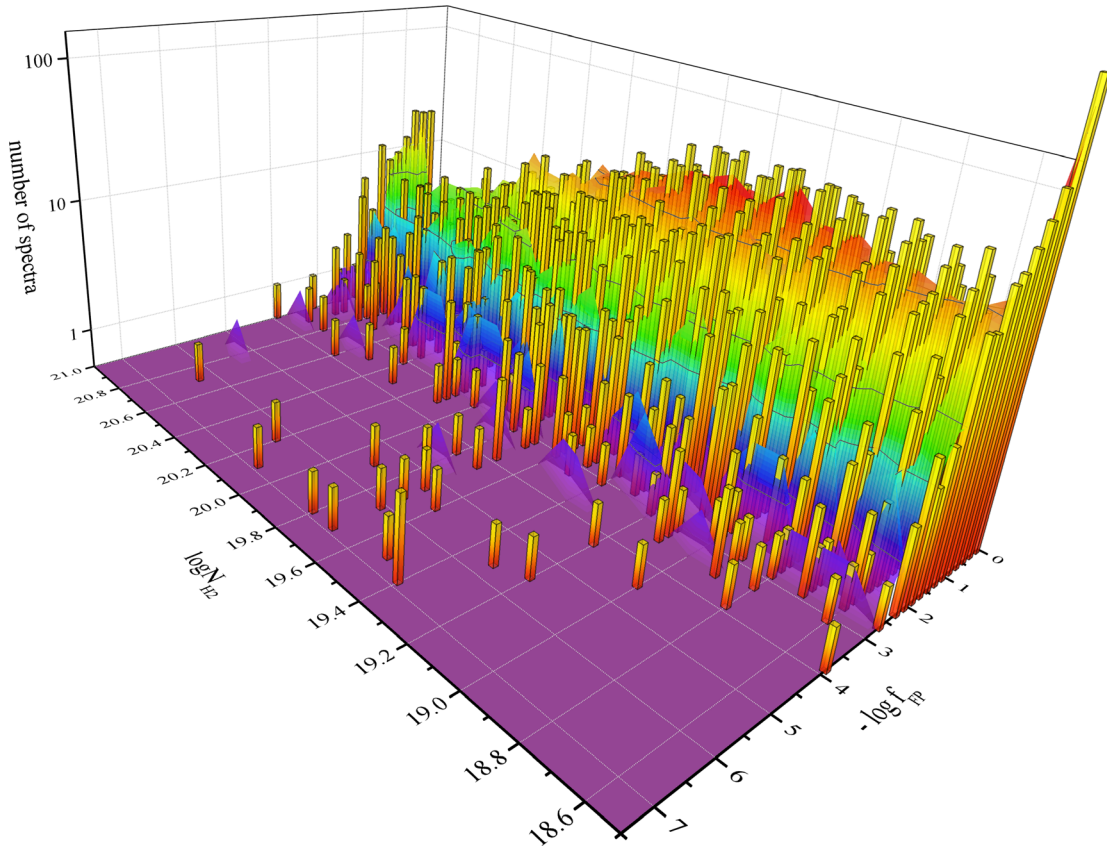
Figure 4. The distributions of f_{FP} values versus the column density of the H_2 absorption system candidates. The orange columns show the calculated distribution using the S_{DLA} sample (where H_2 systems are to be found), while smooth profiles show the distribution calculated from the S_{nonDLA} control sample (where no H_2 systems are expected). The value of $\log(f_{FP}) = -3$ can be considered as the threshold for robust identification, since there are only a few spectra from the S_{nonDLA} control sample with smaller f_{FP} values.

The value of f_{FP} gives an estimate of the FIP for the candidate. However H_2 absorption lines have rigid relative position, while in the above calculation of f_{FP} we used random relative positions to increase statistics. We note that applying random shifts to H_2 absorption lines with respect to a fixed Lyα forest is equivalent to applying random shifts to Lyα forest lines with respect to fixed H_2 absorption. The latter would be difficult to realize technically, therefore, we shifted H_2 absorption lines from their positions. Nevertheless it is necessary to estimate the f_{FP} value at which the detection can be considered as robust. To do this we used the following steps. We have applied the searching procedure to the SDSS spectra without DLAs. We chose subsample, S'_{nonDLA}, of the control sample S_{nonDLA} with size equal to the size of S_{DLA} sample. For each spectrum with z_{QSO} from the S'_{nonDLA} subsample we have generated the redshift of a 'fictitious' DLA system using the distribution of z_{DLA} in the subsample of S_{DLA} spectra which have QSO redshifts in the range $z_{QSO} \pm 0.1$. The absence of real DLAs in the spectra of S'_{nonDLA} subsample guarantees that there is no H_2 absorption system in the spectrum. We searched for 'H_2 candidates' in this sample which are almost certainly false identifications. For each of the selected 'H_2 candidate' we have calculated f_{FP}. The distributions of f_{FP} values for the S_{DLA} (indicated as discrete measurements) and S'_{nonDLA} (smooth profiles) samples are shown in Fig. 4 versus the H_2 column densities. It is apparent that a value of $\log f_{FP} < -3$ can be considered as the limit for reliable identification, as there is sufficient excess in the distribution of the candidates from the S_{DLA} sample.

4.2 Use of a control sample

The FIP of an H_2 absorption system can be estimated as the rate of identifications in spectra where no H_2 absorption system is expected.

FIP mainly depends on the quality of the spectrum, density of the Lyα forest and certain profile of H_2 absorption system. We took four parameters (which we found enough) to describe this dependence: z_{QSO}, S/N, N_{H_2} and the number of H_2 absorption lines that can be seen in the spectrum. We characterize the latter by the parameter $\lambda_B = \lambda_{cut-off}/(1 + z_{DLA})$ which is the blue limit of the spectrum expressed in the DLA rest frame. H_2 absorption lines have rest wavelength $\lambda < 1110$ Å. In order to detect at least one H_2 line, λ_B must be < 1110 Å. FIP has to be determined at each combination of these parameters. We have calculated FIP on a grid of H_2 column densities, S/N, λ_B and z_{QSO} parameters values. Log(S/N) was considered from 0.2 to 1.4 by step of 0.1. The different values of λ_B were taken to correspond to an increment in the number of H_2 lines. The redshift of QSO, z_{QSO}, was varied in the range from 2.2 to 4.2 with 0.4 step.

For each spectrum in the S_{nonDLA} control sample we chose randomly several positions of z_{DLA}. Each of z_{DLA} for the spectrum corresponds to different number of H_2 absorption lines involved in analysis, or λ_B bin. Therefore one spectrum can be used several times with different z_{DLA}. In other words, we constructed enlarged sample S'_{nonDLA}, which allowed us to sufficiently increase statistics. Then we have applied the searching procedure (see Section 3.2) to
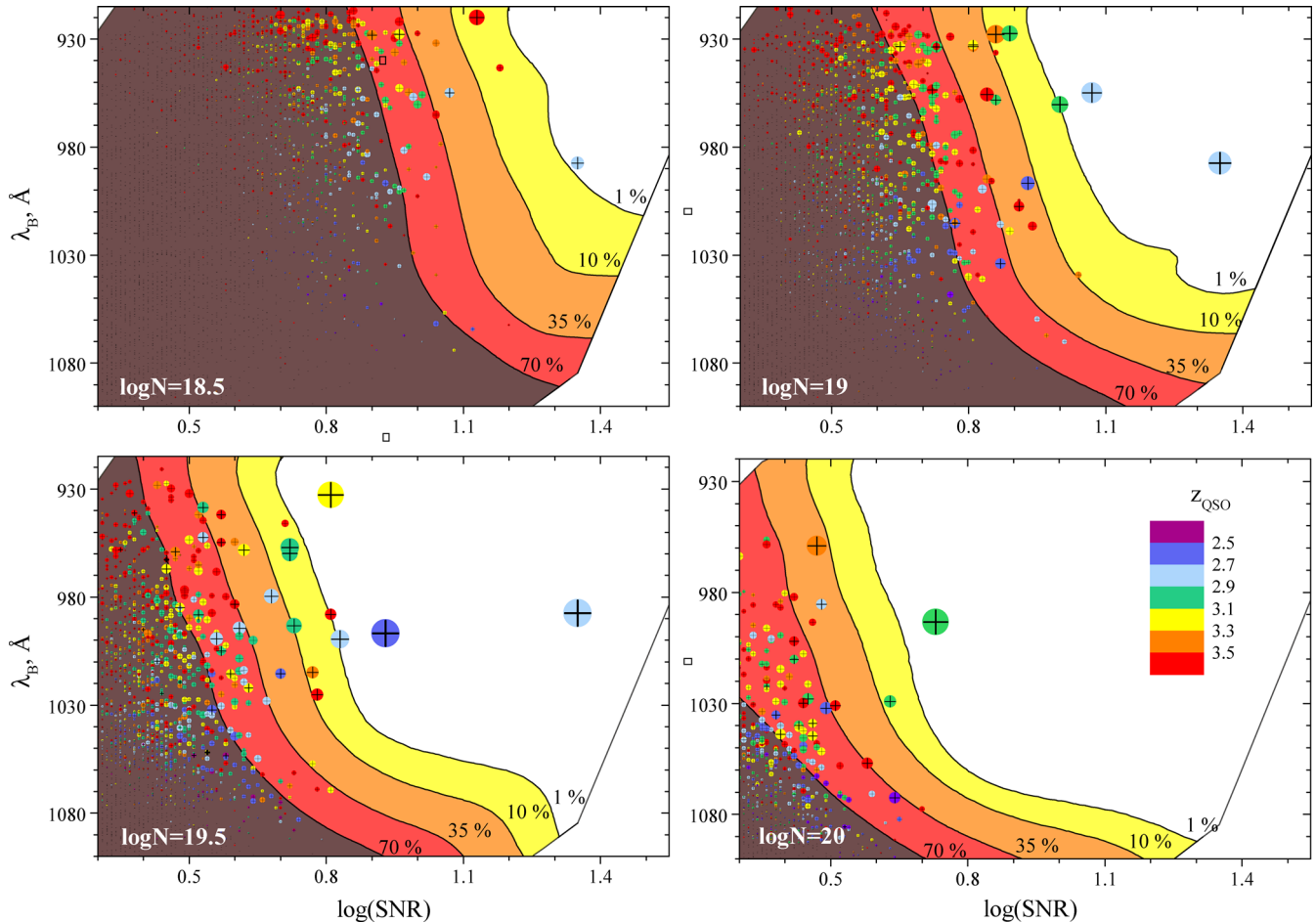
Figure 5. Contour plots of FIP of H_2 absorption systems estimated by using the control sample S'_{nonDLA}. The different panels show f_{CS} for different $\log N$ – the total H_2 column density. *Y*-axis correspond to λ_B – a parameter characterizing the number of H_2 bands available. *X*-axis corresponds to the S/N of the spectrum. The white, yellow, orange, red and brown regions correspond to FIP values <1, <10, <35 and <70 per cent, respectively. The black crosses show our candidates H_2 absorption systems. The size of each cross corresponds to the value of f_{FP} estimated from the Monte Carlo method. The bigger the size, the lower the f_{FP} value. The colour of each cross corresponds to the redshift of the candidates.

enlarged sample S'_{nonDLA} and have calculated the identification rate for each H_2 column density in the selected S/N and λ_B bins:

$$f_{CS}(\lambda_B, S/N, z_{QSO}, N_{H_2}) = n(L < L_{id})/n_{bin}, \qquad (4)$$

where $n(L < L_{id})$ is the number of spectra in the bin, for which the identification criterion ($L < L_{id}$) is satisfied, n_{bin} is the total number of spectra in the bin. The identification rate in the S_{nonDLA} sample gives us the estimate of the FIP. The contour plots of f_{CS} for different N_{H_2} are shown in Fig. 5. f_{CS} depends mainly on λ_B and S/N and little on z_{QSO}. Therefore to construct the contour plots we integrated f_{CS} over the z_{QSO} bins. The dependence of FIP, f_{CS}, on z_{QSO} is shown in Fig. 6. Note that the contour plots shown in Figs 5 and 6 are smoothed over the bins. The general behaviour of f_{CS} satisfies reasonable expectations. The probability decreases with decreasing λ_B (i.e. increase of the number of available H_2 lines), and with increasing S/N and decreasing z_{QSO} (forest less dense). Additionally, the probability decreases with increasing total H_2 column density N_{H_2}.

The calculated identification rate f_{CS} gives an upper limit on the FIP of H_2 absorption system. Indeed, we searched H_2 system in some redshift window around z_{DLA}. The probability that at some redshift in the search window identification criterion to be satisfied increase with increase of search window width. Therefore the rate

f_{CS} is scaled with changing the search window width. The rate f_{CS} approaches FIP value with reducing search window width. However, we cannot set search window very small since we do not know the exact position of H_2 system relative to z_{DLA} (which sets the centre of the search window).

To estimate the FIP of our H_2 candidates derived from the S_{cand} sample we have to position the corresponding spectra in Fig. 5. The candidates can be seen as crosses. The size of each cross indicates the calculated FIP from the Monte Carlo method (see Section 4.1). Note that the FIP estimated from the two methods are in agreement. It is apparent that the overwhelming majority of candidates are located in regions where the FIP probability is high, i.e. these identifications are not robust. However, some spectra are located in regions with low FIP.

Using these considerations, we can estimate the thresholds in S/N and λ_B for robust identification at a given N_{H_2} at some f_{CS} level. We note that the detection limit of H_2 absorption systems in SDSS spectra is higher than $\log N \sim 19$. Indeed, it is seen from Fig. 5 that for confident detection, $f_{CS} < 10$ per cent, of H_2 absorption system with column density $\log N \sim 19$ the high S/N spectrum is required. Such spectra are very rare in SDSS data base.

Sample S'_{nonDLA} has a limited number of spectra in some bins of the parameter space, especially at high S/N and low λ_B value.
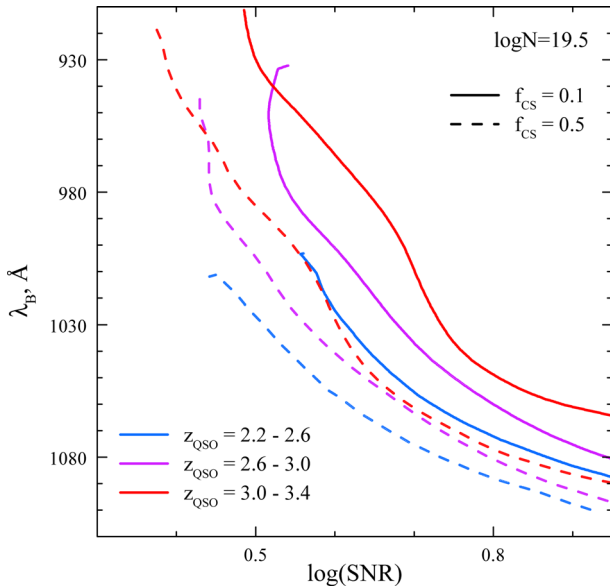

Figure 6. Dependence of the f_{CS} (the upper limit on the FIP) on z_{QSO}. Solid and dashed lines show the f_{CS} isocontours at 0.1 and 0.5, respectively. The f_{CS} is calculated for $\log N(H_2)(cm^{-2}) = 19.5$. Blue, purple and red lines correspond to f_{CS} calculated using spectra with z_{QSO} in the ranges (2.2–2.6), (2.6–3.0) and (3.0–3.4), respectively.

Additionally we have used each spectrum several times. Therefore, we used simulated spectra to check the influence of these limiting factors. We generated a $S_{Ly\alpha}$ sample quasar spectra. The overall shape of the continuum was constructed using principal component coefficients from Pâris et al. (2011) (we used only the 10 first PCA coefficients). The Lyα forest column density and Doppler parameter distributions and the evolution with redshift of the number density were taken from Meiksin (2009). The initial spectrum was calculated at high resolution ($>100\,000$) and then convolved with the SDSS BOSS instrumental function taken from Smee et al. (2013). Finally, we added Poisson noise corresponding to the SDSS sample. We generated a substantial number of spectra (~ 400) in each bin of λ_B and S/N. We applied our searching procedure and calculated the identification rate in each bin. We find that f_{CS} estimated from the SDSS DR9 sample and from the mock sample generally are agree within statistical errors.

4.3 Probability of H$_2$ detection in DLAs

The FIP estimated in the previous section allows us to determine the probability of H$_2$ detection in DLAs. For each column density we have selected the regions of the λ_B–S/N parameter space (shown in Fig. 5) where f_{CS} is less than a given threshold value. In principle it is better to use as low threshold value as possible, because this reduces possible biases and increases the robustness of the detection. However, in order to increase statistics, we have taken a threshold value of 50 per cent. We checked that lower threshold values give consistent results, with larger statistical errors. In each bin of the λ_B–S/N parameter space we compared the identification rates of H$_2$ absorption systems in the S_{DLA} and S'_{nonDLA} samples. The probability of detection of H$_2$ systems with column density larger than a given value N_{H_2} can be calculated as

$$P(N_{H_2}) = \frac{\sum N_{S_{DLA}}(f_{CS}(S_{DLA}) - f_{CS}(S'_{nonDLA}))}{\sum N_{S_{DLA}}}, \quad (5)$$
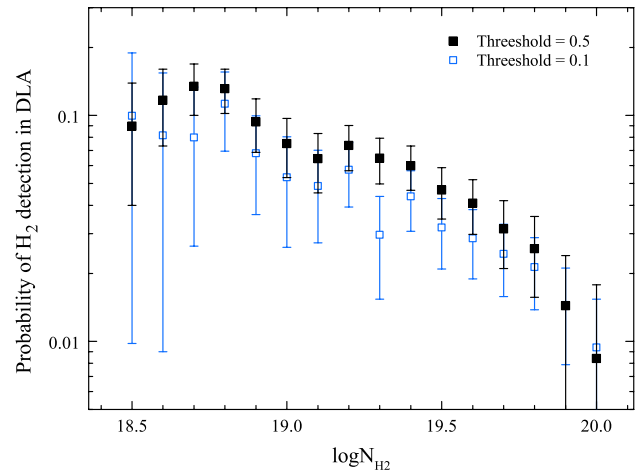

Figure 7. Detection probability of H$_2$ absorption systems in DLAs versus column density. Note that this probability should be considered as an upper limit because our H$_2$ column densities are generally overestimated. Blue open and black filled squares correspond to the calculation with 0.1 and 0.5 threshold values of the detection rate, respectively.

where sums are taken over the bins with $f_{CS}(S'_{nonDLA})$ less than some threshold value, and $N_{S_{DLA}}$ is the number of spectra with DLAs in the bin, $f_{CS}(S_{DLA})$ and $f_{CS}(S'_{nonDLA})$ are the detection rates of H$_2$ absorption systems in the bin in the S_{DLA} and S'_{nonDLA} samples, respectively. The results of the calculation for two threshold values are shown in Fig. 7. The higher threshold values give larger statistics and therefore smaller error bars. However, calculation using higher threshold values lead to higher values for obtained probability, which is seen in Fig. 7. Nevertheless, the results of the calculation for threshold values 0.1 and 0.5 are in the agreement with each other. Note that this probability, especially at the low column densities, should be considered as an upper limit because our procedure tends to overestimate the column density due to the quality of SDSS spectra.

Based on the Very Large Telescope (VLT) survey of H$_2$ absorption systems in QSO spectra (Noterdaeme et al. 2008a) it was found that the overall covering factor of H$_2$ in DLAs is ~ 10 per cent for $\log f > -4.5$. For the high end of the $N(H_2)$ as considered here, the VLT survey indicates rather 8 per cent ($N(H_2) > 18$) or less, in very good agreement with our analysis.

5 CANDIDATES

We have compiled the final sample, S_{final}, of the most promising H$_2$ candidates for follow-up studies. Fig. 8 shows the f_{FP} and f_{CS} values calculated for each candidate in the S_{cand} sample by the two methods presented in Sections 4.1 and 4.2, respectively. As we stated above f_{CS} calculated using the control sample gives an upper limit on the FIP, as it depends on the width of the search window. In turn f_{FP} estimated using Monte Carlo simulations gives a lower limit on FIP. Nevertheless it is seen again that Monte Carlo sampling and control sample methods are in agreement with each other. The S_{final} sample presented in Table 1 is formed from new H$_2$ candidates which have $\log f_{FP} < -3$ (see Fig. 4) and $f_{CS} < 0.1$. The selected candidates are shown in Fig. 8 by red circles. The known H$_2$ absorption systems shown in Fig. 8 by blue points were excluded from the S_{final} sample and not listed in Table 1. The filled and open circles in Fig. 8 correspond to candidates from DR9 and DR7, respectively. We found that improved quality of quasar spectra
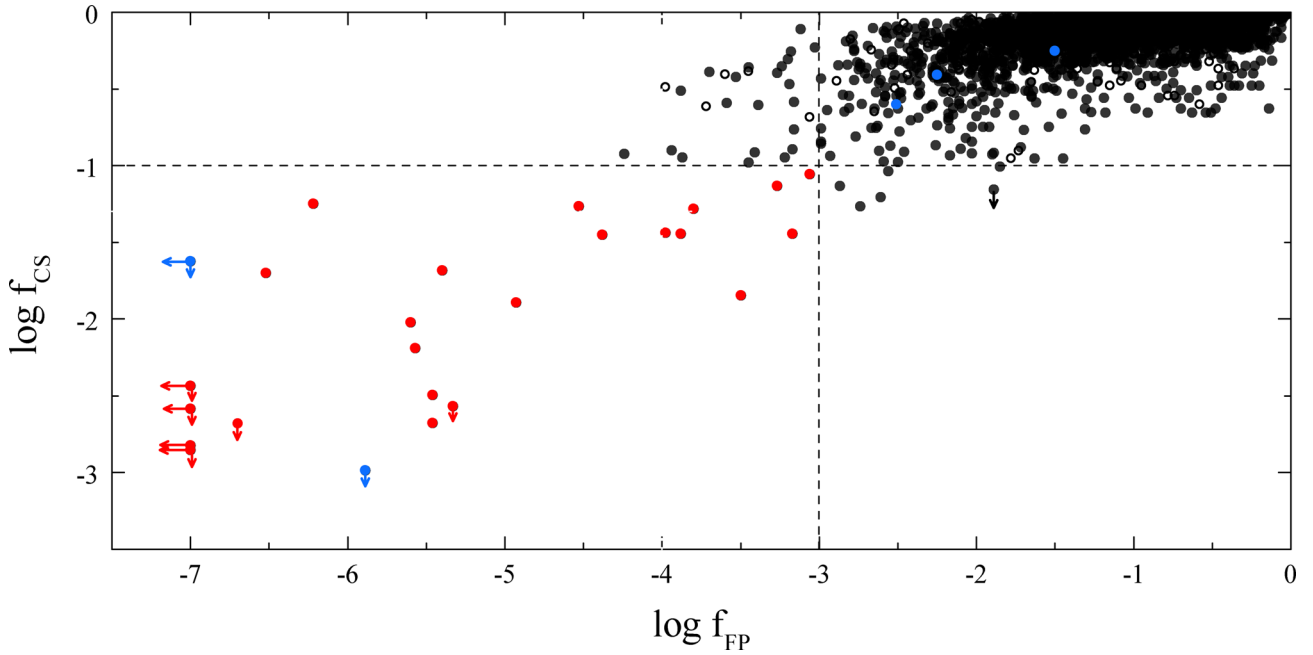
Figure 8. The outputs of the two methods used to estimate the confidence level of H$_2$ candidates are used to select the final sample. Red circles show selected H$_2$ candidates. Filled and open circles correspond to candidates from DR9 and DR7, respectively. Blue circles show the known H$_2$ absorption systems. Two of them (J081240.69+320808.52 and J123714.61+064759.64) are easily found by our method.

Table 1. The S_{final} sample of new H$_2$ absorption system candidates in SDSS-DR9. Here z_{em}, z_{DLA} and log $N_{\mathrm{H\,I}}$ (cm^{-2}) are quasar and DLA system redshifts and column density of H I taken from Noterdaeme et al. ([2009](#)), S/N is log of estimated signal-to-noise ratio of the spectrum in the region where H$_2$ lines should be seen, λ_{B} is wavelength of the cut-off in the spectrum in the DLA rest frame, log $N_{\mathrm{H_2}}$ (cm^{-2}) is estimated upper limit on the H$_2$ total column density, T_{01}, (K) is kinetic temperature which gives the relative population of J = 0, J = 1 H$_2$ rotational levels, f_{FP} is the probability of false detection estimated by Monte Carlo sampling, see Section 4.1, f_{CS} is the probability of false detection estimated by control sample expressed in per cent, see Section 4.2, Δ_V (km s^{-1}) is the difference between redshifts of H$_2$-bearing component and DLA system (measured by metal lines).

Quasar	Plate-MJD-fibre	z_{em}	z_{DLA}	log $N_{\mathrm{H\,I}}$	S/N	λ_{B} (Å)	log $N_{\mathrm{H_2}}$	T_{01}	log (f_{FP})	f_{CS}	Δ_V
J234730.76−005131.68	4214-55451-0212	2.63	2.5874	20.20	0.9	996	19.5	25	< -7.0	0.1	−60
J221122.52+133451.24	5041-55749-0374	3.07	2.8376	21.85	0.7	993	20.1	25	< -7.0	<0.1	−70
J114824.26+392526.40	4654-55659-0094	2.98	2.8320	20.84	1.0	960	19.4	25	< -7.0	<0.3	−30
J075901.28+284703.48	4453-55535-0850	2.85	2.8221	20.87	1.1	955	19.2	25	< -7.0	<0.4	−70
J153134.59+280954.36	3959-55679-0862	3.23	3.0025	21.01	0.8	932	19.5	25	-6.7	<0.2	60
J001930.55−013708.40	4366-55536-0874	2.53	2.5284	20.64	0.5	1032	20.7	25	-6.5	2.0	−130
J152104.92+012003.12	4011-55635-0218	3.31	3.1410	21.56	0.5	958	20.2	25	-6.2	5.6	−150
J013644.02+044039.00	4274-55508-0691	2.81	2.7787	20.47	0.7	979	19.7	25	-5.6	1.0	−110
J105934.34+363000.00	4626-55647-0381	3.77	3.6402	20.97	0.8	955	19.3	25	-5.6	0.7	−80
J164805.16+224200.00	4182-55446-0880	3.08	2.9900	21.52	0.7	957	19.6	25	-5.5	0.3	−40
J160638.54+333432.89	4965-55721-0091	3.09	3.0845	20.42	0.9	927	19.2	25	-5.5	0.2	−80^a
J123602.11+001024.60	3848-55647-0266	3.03	3.0289	20.58	0.5	938	19.9	25	-5.4	2.1	−420^b
J144132.27−014429.40	4026-55325-0848	2.98	2.8908	21.46	0.7	959	19.7	25	-5.3	<0.3	110^a
J150739.67−010911.16	4017-55329-0647	3.10	2.9743	20.05	0.6	958	19.8	25	-4.9	1.3	−30
J150227.22+303452.68	3875-55364-0040	3.33	3.2828	20.83	0.9	927	19.0	25	-4.5	5.5	0
J082102.66+361849.68	3760-55268-0364	2.81	2.8030	20.38	0.6	994	19.7	25	-4.4	3.5	−10
J084312.72+022117.28	3810-55531-0727	2.91	2.7866	21.80	0.4	1040	21.0	25	-4.0	3.6	−10
J123052.64+020834.80	4752-55653-0116	3.36	2.7981	21.26	0.8	1015	19.7	25	-3.9	3.6	20
J082716.26+395742.48	3761-55272-0810	2.83	2.7420	20.59	1.0	956	18.8	25	-3.8	5.2	50
J004349.39−025401.80	4370-55534-0422	2.96	2.4721	20.57	0.6	1029	20.1	25	-3.5	1.4	270^c
J120847.64+004321.72	3845-55323-0604	2.72	2.6083	20.35	1.0	993	18.8	25	-3.3	7.4	−40
J160332.00+081622.44	4893-55709-0876	2.86	2.8429	20.27	0.9	942	18.9	25	-3.2	3.6	−10
J141205.80−010152.68	4035-55383-0704	3.75	3.2678	20.53	0.9	1007	19.1	25	-3.1	8.8	30

^{a}C I metal lines are tentatively detected in these spectra. It is believed that C I is a good tracer of H$_2$.
^{b}In this DLA system H$_2$-bearing component associated with the second, less prominent component in metal line profile.
^{c}Low-ionization metal lines are not detected in this system. z_{DLA} estimated using C IV and Si IV metal transitions. Visual inspection showed that this candidate is unlikely.

in SDSS-III has major importance for detection of H_2 absorption systems. There are only two candidates (J081240.69+320808.52 and J153134.59+280954.36) in DR7 satisfied the selection criterion for S_{final} sample ($\log f_{FP} < -3$ and $f_{CS} < 0.1$). They were both re-observed and presented DR9 catalogue thus we used its DR9 spectra.

Note that the H_2 column densities given in Table 1 are generally overestimated. This arises mainly from two factors. The first is the numerous blends in the Lyα forest which can be unresolved at the resolution of SDSS spectra. The second is that our procedure gives the highest column density for which the criterion of detection, $L < L_{id}$, is satisfied. We found that SDSS data quality is not high enough to estimate with reasonable uncertainty H_2 column densities using standard χ^2 likelihood profile fitting. Using simulations of SDSS mock spectra with specified H_2 absorption systems we can estimate that the standard χ^2 procedure gives systematic errors larger than 0.5 dex.

High-resolution spectrum studies of H_2 absorption systems ($\log N \gtrsim 19$) indicate that H_2-bearing DLAs are usually associated with prominent metal lines. We found that the redshifts of H_2-bearing component of the candidates are satisfied with redshifts of DLA system within 100 km s^{-1}, which is less than errors in the redshift determinations. Only in two of the H_2 candidates (see Table 1, they marked by superscript a) we have detected C I absorption lines which are known as a good tracer of molecules (Srianand et al. 2005; Noterdaeme et al. 2012). Detections of C I are rare in SDSS spectra as a consequence of the low resolution of the spectra.

For instance, we present two candidates in the spectra of J234730.76−005131.68 and J084312.72+022117.28 in Figs 9 and 10, respectively. The J234730.76−005131.68 spectrum has relatively high S/N and the candidate has very low f_{FP} value, i.e. the detection of the H_2 absorption system is robust. The J084312.72+022117.28 spectrum has lower S/N and the candidate higher f_{FP} value, but from Fig. 10 it can be seen that highly saturated H_2 absorptions are prominent. The estimated column density of this

H_2 candidate is $10^{21.1}$ cm^{-2}. Such high H_2 column densities have never been observed towards high-redshift quasars. There are also three candidates in Table 1, which have estimated column densities exceeding 10^{20} cm^{-2}. Such saturated H_2 systems are detected up to now only towards two GRBs (Prochaska & Wolfe 2009; Krühler et al. 2013), and are usual in our Galaxy (Rachford et al. 2002). These four selected highly saturated H_2 systems are very promising candidates to probe the translucent phase of high-redshift ISM.

Table 2 gives the properties of seven H_2 absorption systems that were previously identified from high-resolution spectra obtained at Keck and/or VLT observatories. One of them (J143912.04+111740.5) was not included in the DLA catalogue due to poor S/N, but we included the spectrum in the searching sample, S_{DLA}. For two of them H_2 lines fall out the searched region due to poor spectral quality. We identify the H_2 absorption systems in all of the five remaining spectra. However, the identification is robust only for two systems. They have $\log N_{HR}(H_2) > 19$ measured from high-resolution data. For the other three systems (J144331.17+272436.73, J081634.39+144612.36 and J235057.87−005209.84) with H_2 column density $\log N_{HR}(H_2)$ lower than 19, our FIP is not low enough $>10^{-3}$, i.e. identification is not robust and they cannot be considered as reliable candidates.

6 PROPERTIES OF H_2 CANDIDATE SAMPLE

In this section we present the properties of candidates in the S_{final} sample. The main goal is to search for difference between the properties of H_2-bearing and non-H_2-bearing DLAs. The distributions of neutral hydrogen column density for H_2 candidate sample and DLA sample are shown in Fig. 11. The Kolmogorov–Smirnov test indicates that we can reject the hypothesis that the two distributions are the same at the 0.99 level. Comparison of the distributions shows that the presence of high column density H_2 absorption systems leads to the higher H I column densities.
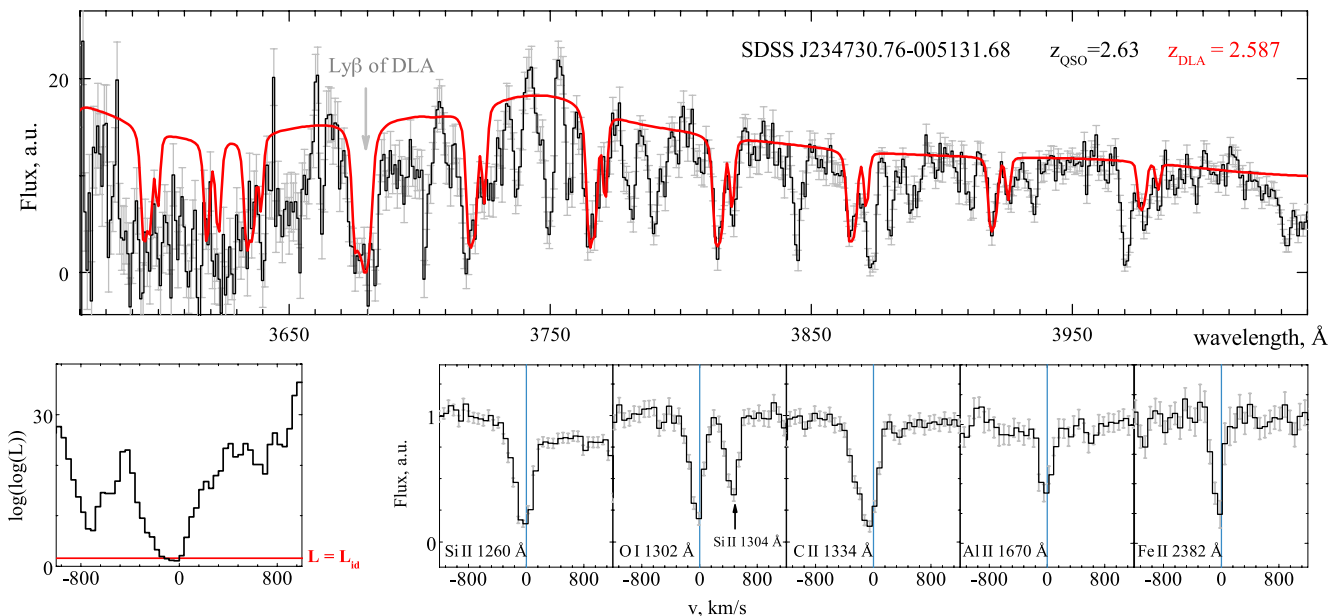

Figure 9. The spectrum of SDSS J234730.76−005131.68. The top panel shows part of the spectrum with fitted H_2 profiles at $z = 2.587$ overplotted. The five right-hand bottom panels show metal lines associated with this system. Left-hand bottom panel shows the dependence of the searching criterion with redshift, expressed as a velocity offset from the position of the system.
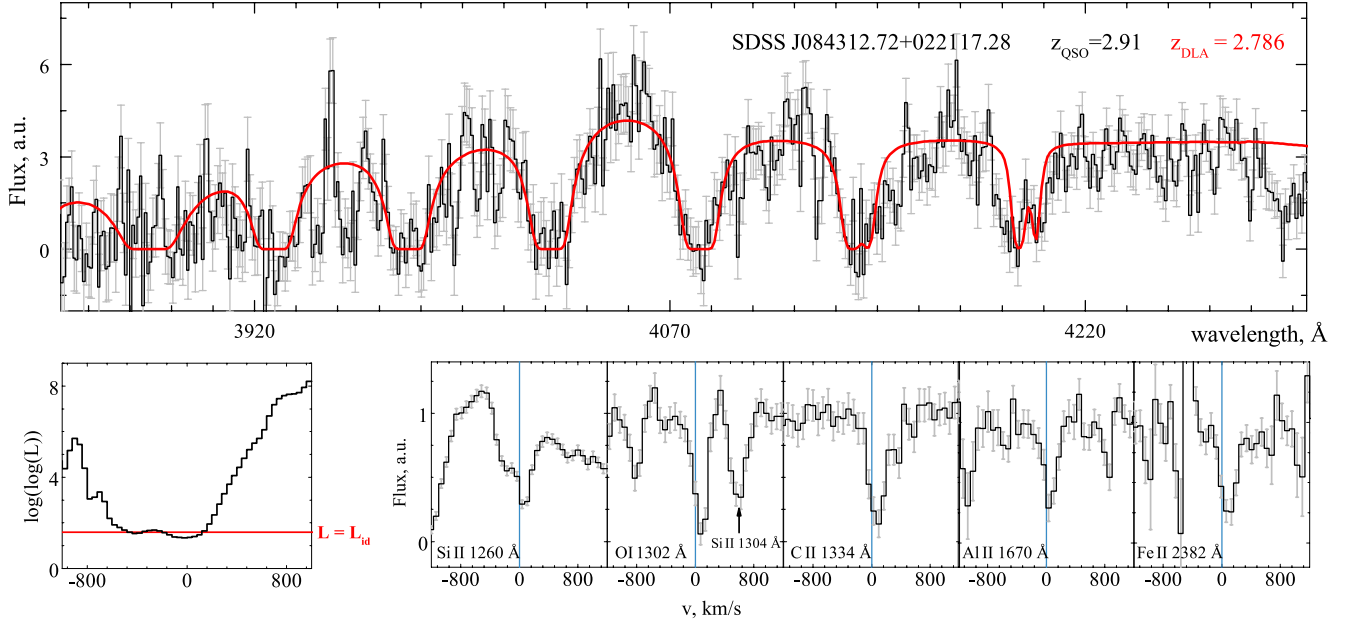
Figure 10. The candidate in the spectrum of SDSS J084312.72+022117.28 has possibly the highest column density ever detected in front of QSOs, $\log N_{H_2} = 21.1$. The top panel shows part of the spectrum with fitted H_2 profiles. The five right-hand bottom panels show metal lines associated with this system. Left-hand bottom panel shows the dependence of the searching criterion with redshift, expressed as a velocity offset from the position of the system.

Table 2. Already known H_2 system in SDSS. $\log (f_{FP})$ is an estimate of FIP, estimated by Monte Carlo sampling method. $\log N$ is the H_2 column density estimated by our procedure. $\log N_{HR}$ is H_2 column density known from analysis of high-resolution spectrum.

Quasar	z_{em}	z_{abs}	$\log (S/N)$	$\log (f_{FP})$	$\log N$	$\log N_{HR}$	Instrument	Comment	Ref.
J081240.69+320808.52	2.70	2.625	1.4	<-7.0	19.8	19.88 ± 0.06	KECK/HIRES	HD	a
J123714.61+064759.64	2.79	2.689	0.8	-5.5	19.9	$19.21^{+0.13}_{-0.12}$	VLT/UVES	Multicomp, HD/CO	b
J144331.17+272436.73	4.44	4.225	0.6	-2.5	19.2	18.29 ± 0.08	VLT/UVES		c
J081634.39+144612.36	3.85	3.287	0.6	-1.7	19.8	$18.66^{+0.17}_{-0.30}$	VLT/UVES	Multicomp	d
J235057.87−005209.84	3.02	2.425	0.6	-1.4	19.7	$18.52^{+0.30}_{-0.49}$	VLT/UVES	Multicomp	e
J143912.04+111740.5	2.58	2.418	0.6	Out of range		19.38 ± 0.10	VLT/UVES	Multicomp, HD/CO	f
J091826.16+163609.0	3.07	2.58	0.1	Out of range		19/16	VLT/X-shooter	Not in DLA sample	g

Note. Ref.: a – Jorgenson et al. (2009), b – Noterdaeme et al. (2010), c – Ledoux, Petitjean & Srianand (2006), d – Guimarães et al. (2012), e – Petitjean et al. (2006), f – Srianand et al. (2008), g – Fynbo et al. (2011).

6.1 Colour excess

We have studied the colour excess for the H_2 candidate sample, S_{final}. Recently it was shown that quasar spectra with H_2/CO-bearing absorption systems show significant $g - r$ colour excess compared to quasar spectra with non-molecular bearing DLAs (e.g. Noterdaeme et al. 2010). This excess might be caused by (i) the presence of H_2 absorption lines in H_2 candidate spectra; (ii) the increased dust content of the H_2-bearing DLA (because H_2 molecules in the cold neutral medium mainly form on to the dust grains). To estimate the colour excess we used the following procedure. SDSS filters magnitudes were taken from the DR9 quasar catalogue (Pâris et al. 2012). For each H_2 candidate we have selected a control sample of quasars from the DR9 catalogue with redshifts similar to redshift of the candidate quasar (within $\Delta z = 0.05$). We have compared the value of $r - i$ colour for each candidate with the median value of $r - i$ in the control samples (the top right- and left-hand panels of Fig. 12). In comparison with previous studies we have chosen r and i filters because there is no bias due to the presence of H_2 absorption lines. Using dispersions measured in the control samples we have calculated standard deviations of the candidates from their control

samples (the middle left-hand panel of Fig. 12). We have found 1σ excess in the $r - i$ colours for H_2 candidate sample from their control samples. Additionally, we have found that $r - i$ colour excesses for H_2 candidates are statistically higher than colour excesses measured for the DLA sample (for this purpose we used the statistical DLA sample from Noterdaeme et al. 2012, which is a subsample of S_{DLA} sample), see Fig. 13. Since H_2 absorption lines for H_2 candidate do not fall in r and i SDSS filters we suppose that this excess is the evidence of enhanced dust content in H_2-bearing DLAs. We found significant excesses of H_2 candidate sample over DLA sample in $g - r$, $u - r$, $r - z$ colours as well. The excesses in $g - r$, $u - r$ colours are about 2σ of standard deviation that are higher than $\sim 1\sigma$ excesses measured in $r - i$, $r - z$ (see Fig. 14). It agrees with previous statement about higher extinction in H_2-bearing candidates, but can be also explained by location of H_2 absorption lines over g and u SDSS filters. Fig. 14 shows comparison of standard deviations from their control samples of H_2 candidate and DLA samples, calculated for $g - r$ and $r - z$ colours. We suppose that measured colour excesses most likely are explained by the higher amount of dust in the H_2-bearing DLAs. The latter can be investigated further by extinction measurement from spectral fitting.
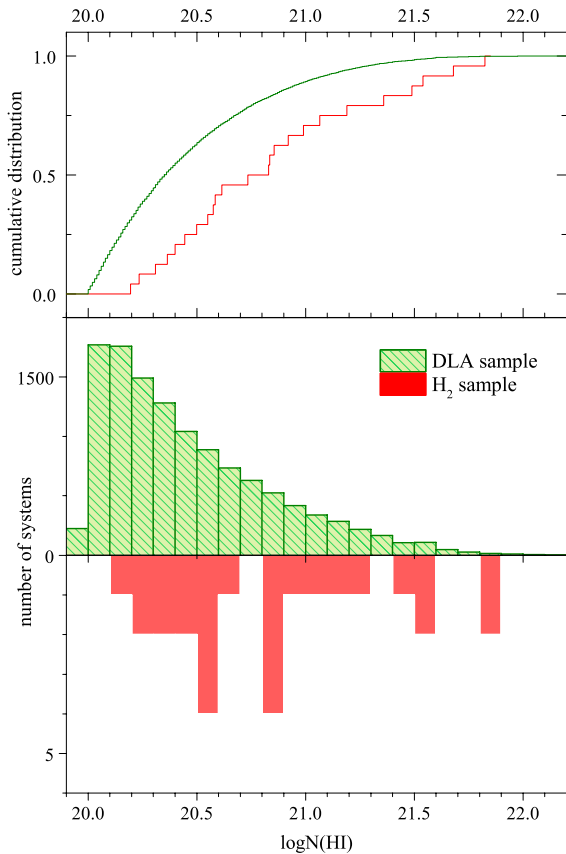
Figure 11. Distribution (bottom panel) and cumulative distribution (top panel) of the column densities of neutral hydrogen in the DLAs. Red and green colours correspond to the sample of H_2-bearing candidates and S_{DLA} sample, respectively.

6.2 Extinction

The 1σ $r - i$ colour excess of H_2 candidates can indicate an enhanced dust content in H_2-bearing DLAs. We therefore perform a direct measurement of extinction of the quasar spectra where H_2 candidates are found. We have used a procedure similar to that used by Srianand et al. (2008) and Noterdaeme et al. (2009). We have corrected the spectra for the Milky Way reddening using A_V maps given in Schlegel, Finkbeiner & Davis (1998) and the improved correction formula by Schlafly & Finkbeiner (2011). We have fitted the QSO continuum of each candidate in the regions without emission lines. The positions of emission lines and initial QSO spectrum were taken from Vanden Berk et al. (2001). We used the Small Magellanic Cloud (SMC)-like extinction curve which was applied at the DLA rest frame. The normalization of the spectrum and A_V were obtained during standard minimization χ^2 fit. For each candidate we have constructed a control sample including non-BAL quasars with no DLA and spectra of $S/N > 3$ and redshifts within $\Delta z = 0.1$ of the redshift of the H_2-bearing candidate QSO. For each quasar of the control sample we measure the virtual extinction that would produce by a DLA at the redshift of the H_2-bearing candidate. Each control sample has a A_V distribution close to normal (an example is shown in the right-hand bottom panel of Fig. 12). The measured median and dispersion of the A_V distribution of the control sample for each candidate is shown as a black point with error bars in the left-hand bottom panel of Fig. 12. The measured A_V values of the H_2 candidates are shown by blue triangles. The

distribution of the deviations (in unit of standard deviation) of A_V in H_2 candidate spectra relative to the median in their control sample is shown in red colour in Fig. 15. The same distribution calculated for the whole DLA sample, S_{DLA}, is shown in blue colour in Fig. 15. Although there is an excess of red colour in the H_2-bearing sample, the Kolmogorov–Smirnov test indicates that we cannot reject that the two distributions are the same (at the 0.41 level). However, note that both samples have 1σ from the control non-DLA non-BAL sample. If this excess is attributed to the dust presence in DLAs, it implies median $A_V \lesssim 0.10$ for DLAs as well as for H_2-bearing system. Such small values of extinction cannot lead to any selection bias for DLAs, which is in agreement with what was found in the radio selected QSO DLA surveys (Ellison et al. 2001; Jorgenson et al. 2006).

6.3 Metal content

The measured EWs of metal transitions can be used to characterize the metal content in DLAs. We used EWs of C II 1334 Å, Si II 1526 Å, Fe II 1608 Å and Al III 1670 Å automatically measured in the DLA DR9 catalogue (Noterdaeme et al. 2012). The distributions of EWs for DLA and H_2 candidate samples are shown in Figs 16 and 17. Note, to construct cumulative distributions in Fig. 17 we used only spectra where metal lines are detected. It rejects most of possible false-positive DLAs which presence in DLA DR9 sample. However, there can be a fraction of DLAs with low metal content, where some metal lines cannot be detected in SDSS spectra. Using Kolmogorov–Smirnov test we have found that EWs in the H_2 candidate sample are higher than EWs in DLA sample for C II 1334 Å, Si II 1526 Å and Al III 1670 Å transitions at significance level 0.001, 0.039 and 0.014, respectively. On the other hand we have found that for Fe II 1608 Å transition distributions of H_2 candidate and DLA samples are not different at 0.94 significance level.

The overall excess in C II, Si II and Al III EWs of the H_2 candidate sample over the DLA sample can possibly be interpreted as evidence for higher metal content. In such an interpretation the corresponding similarity of the Fe II 1608 Å EW distributions could reflect higher dust content in the H_2-bearing systems. However, EWs are not obviously related to column densities at low spectral resolution and large EWs could just be a consequence of larger velocity spread of the absorption. Note however that there is a correlation between velocity spread and metallicity (Ledoux et al. 2006) which would imply larger metallicities in the H_2-bearing candidates.

7 CONCLUSION

We have performed a systematic search for H_2 absorption in DLAs detected towards quasars in the SDSS DR7 and DR9. We have developed and used fully automatic procedures based on the profile fitting technique with modified χ^2 function. The main difficulty of the search is the presence of the Lyα forest which is dense at redshifts under consideration ($z > 2.2$) and can effectively mimic H_2 absorption lines at the resolution and S/N of SDSS spectra. We carefully checked our searching procedure and found that it yields a completeness of >99 per cent for $\log N_{H_2} > 18.5$. However, the number of false detections is rather high. For each of the candidates, the probability of false identification was calculated using two techniques. The first technique employs Monte Carlo simulations to estimate the probability of an accidental fit of an absorption system in the Lyα forest. In this technique we used repeated random shifts for each H_2 absorption line in the particular spectrum. The advantage of this technique is to give an estimate of the FIP
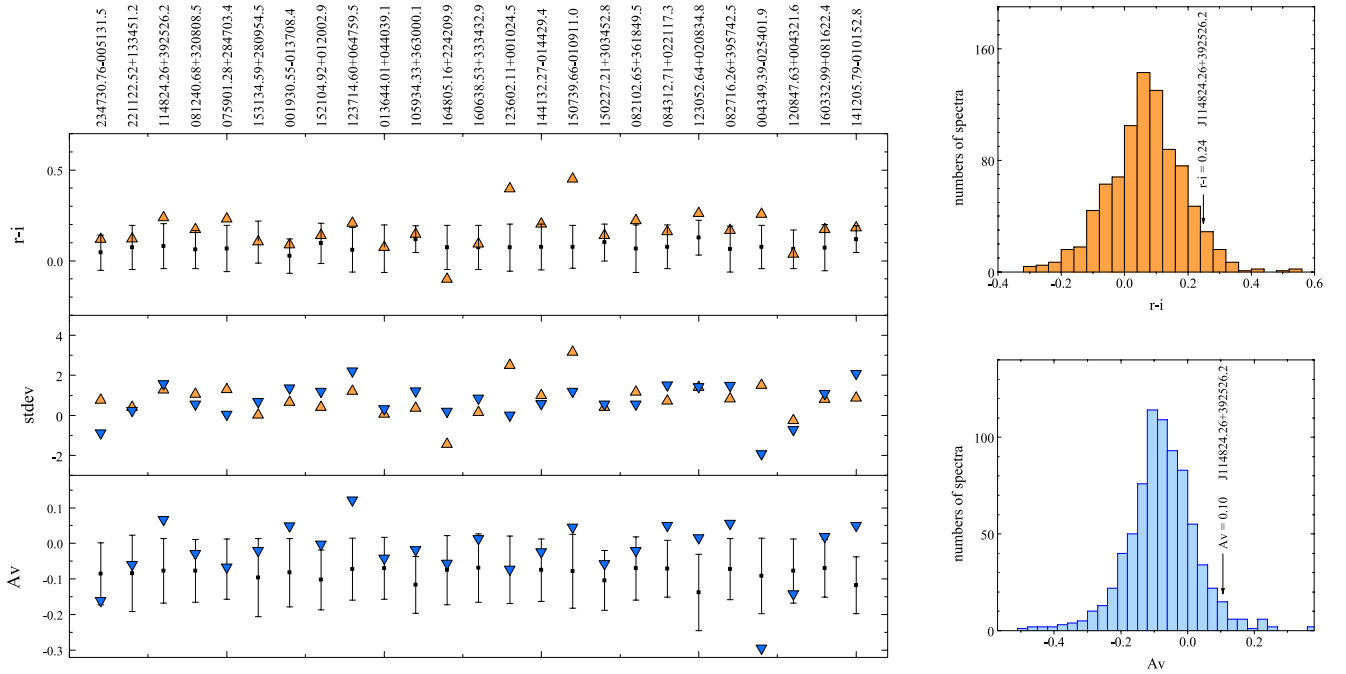
Figure 12. Estimated $r - i$ colours and A_V for selected H₂ candidates. Top left: the orange points in the top left-hand panel show the $r - i$ colour for H₂ candidates while the black points with error bars show the median value and dispersion of $r - i$ colours in control samples for each of the H₂ candidates. Bottom left: the blue points in the top left-hand panel show the A_V for H₂ candidates while the black points with error bars show the median value and dispersion of A_V in control samples for each of the H₂ candidates. Middle left: orange and blue points indicate standard deviation of $r - i$ and A_V, respectively, measured for H₂ candidates from their control sample. Top right: distribution of $r - i$ colour in the control sample of H₂ candidate in J114824.26+392526.2. Bottom right: distribution of A_V in the control sample of H₂ candidate in J114824.26+392526.2.
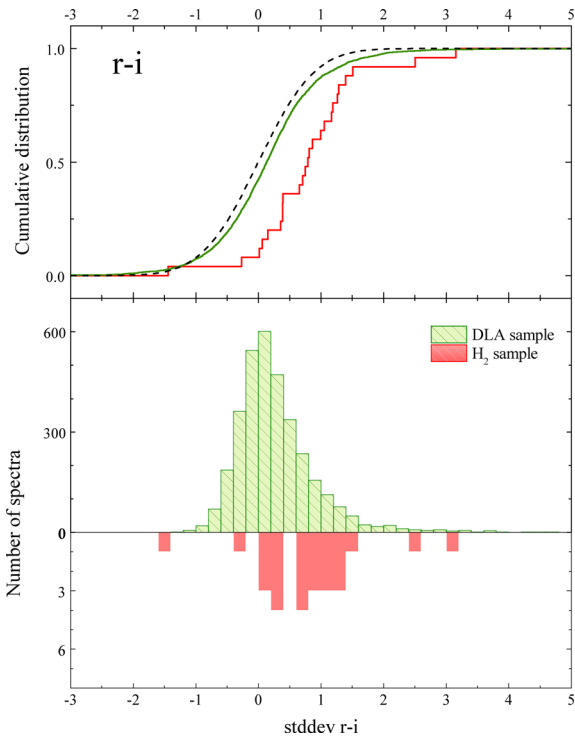

Figure 13. Distribution (bottom panel) and cumulative distribution (top panel) of the standard deviations of $r - i$ compared to the median in the control samples. Red and green colours correspond to the sample of H₂-bearing candidates and DLA sample, respectively. The black dashed line in the top panel shows the cumulative probability for a normal distribution.
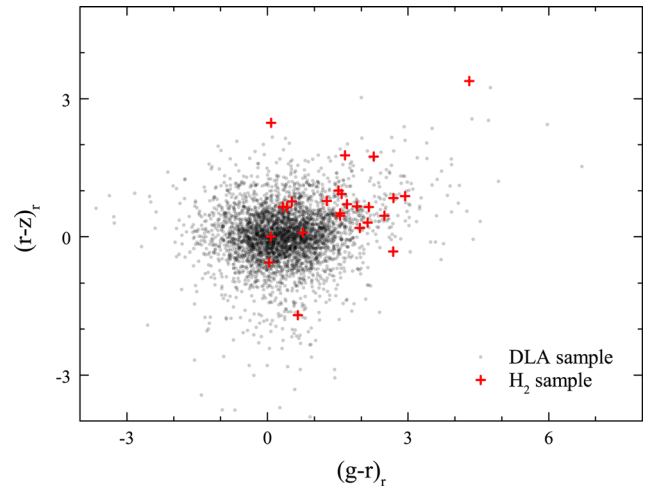

Figure 14. $(r - z)_r$–$(g - r)_r$ colour diagram. Red and black points correspond spectra from the sample of H₂-bearing candidates and DLA sample, respectively. $(r - z)_r$ and $(g - r)_r$ values show $r - z$ and $g - r$ colours measured in standard deviations of their control samples.

in the particular spectrum (i.e. the particular realization of the Lyα forest). The second technique uses a control sample to estimate the FIP. Control sample consists of the non-BAL non-DLA quasars from SDSS DR9 catalogue which guarantees the absence of H₂ absorption systems. The FIP can be calculated as the identification rate of H₂ absorption systems in the control sample. We additionally have performed simulations of mock SDSS quasar spectra which were used to check the procedures and to increase statistics. We have
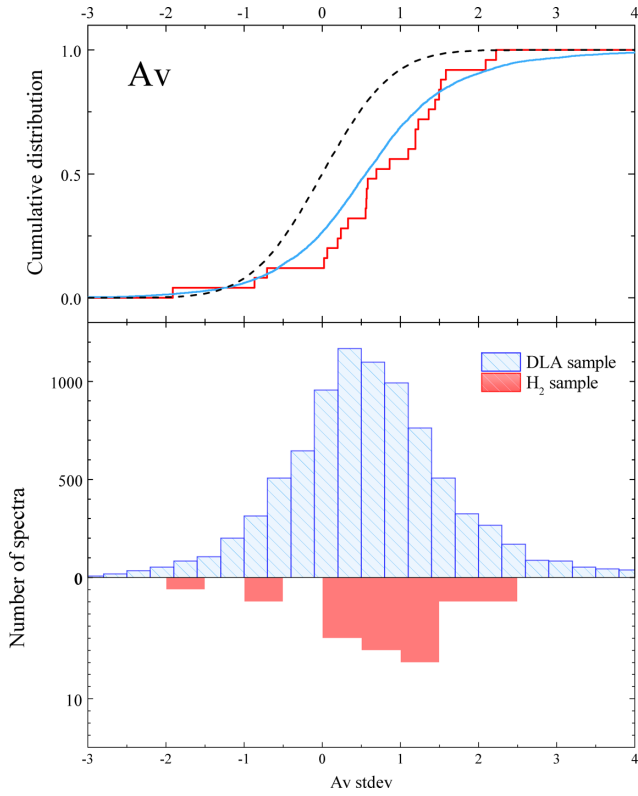
Figure 15. Distributions (bottom panel) and cumulative distributions (top panel) of the deviation (in unit of standard deviation) of A_V compared to the median in the control samples. Red and blue colours correspond to the sample of H_2-bearing candidates and the whole DLA sample, respectively. The black dashed line in the top panel shows the cumulative probability for a normal distribution. A similar excess is seen for the two samples.

found that the FIP depends on the H_2 column density and spectral properties, mainly on S/N, z_{QSO} and the number of H_2 absorption lines present in the spectrum. This method allows us to estimate the detection limit of H_2 absorption systems in SDSS spectra, i.e.
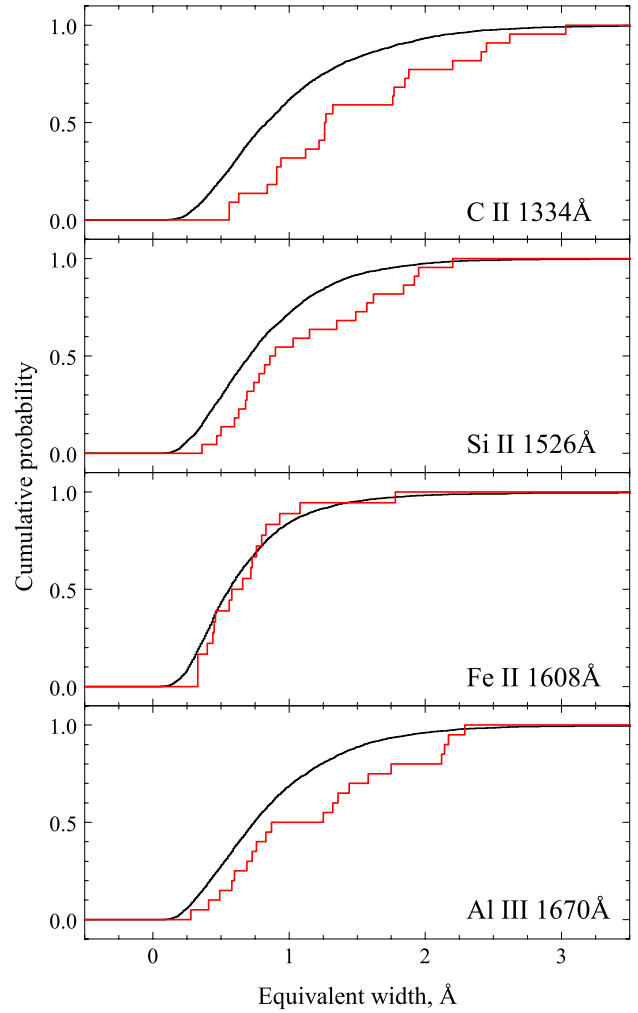

Figure 17. Cumulative distribution of EWs of C II, Si II, Fe II and Al III absorptions. The black and red lines in each panel correspond for samples of DLAs detected in DR9 and H_2 candidates, respectively.
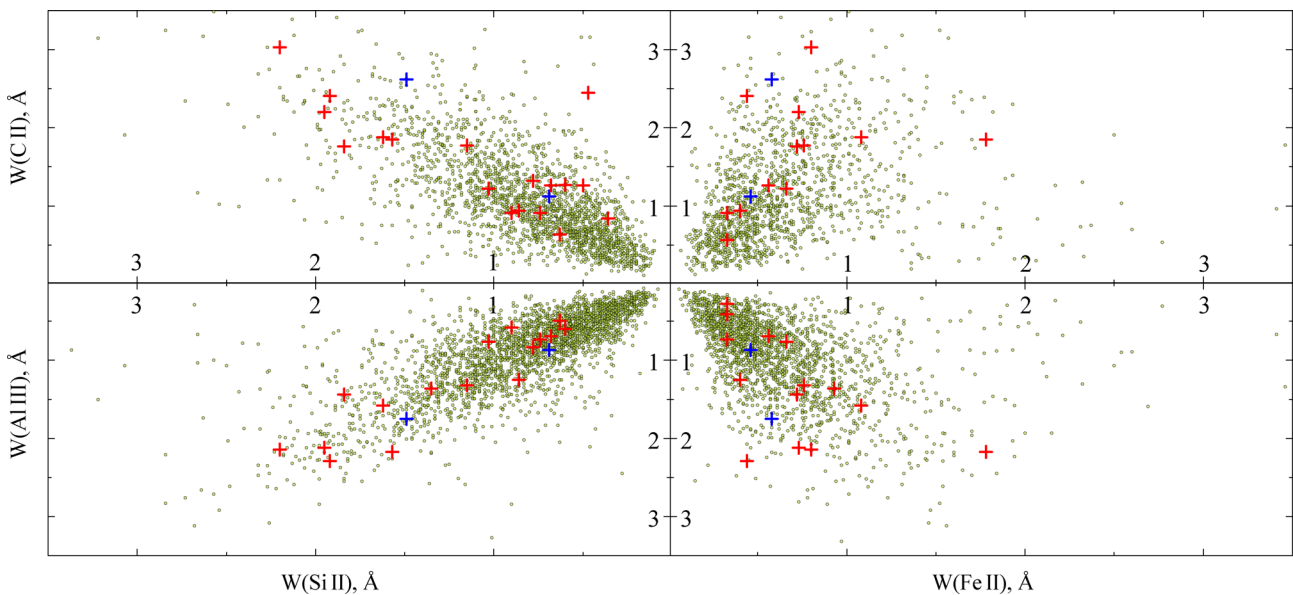

Figure 16. EWs of C II, Si II, Fe II and Al III absorptions. The green circles, red and blue crosses correspond to EWs for DLAs detected in DR9, H_2 candidates and H_2 candidates confirmed by high-resolution studies, respectively.

the spectral properties for which the FIP is low and therefore the identification of the H_2 absorption system is robust. We found that in SDSS data a reasonable detection limit for H_2 column density, $\log N_{H_2}$, is higher than 19. We also derived that the upper limit on the fraction of DLAs with H_2 systems is statistically equal to 7 and 3 per cent for, respectively, $\log N_{H_2} > 19$ and 19.5. These are as upper limits because we tend to overestimate H_2 column densities. The FIPs calculated by the Monte Carlo sampling and control sample techniques agree with each other very well.

We have selected 23 candidates of H_2 absorption systems with high confidence level which are promising candidates for follow-up high-resolution studies. Taking into account the derived upper limit on the fraction of DLAs with saturated H_2 lines ∼7 per cent it leads us to the conclusion that only less than 3 per cent of SDSS spectra are suitable for confident detection of H_2 absorption systems.

We studied the properties of these candidates, namely, colour excess, extinction and EWs of metal lines. There is a $1\sigma\ r - i$ colour excess and no significant A_V extinction in quasar spectra with an H_2 candidate compared to standard DLA-bearing quasar spectra. We find larger C II, Si II and Al III EWs in the H_2 candidate sample over the DLA sample but no significant difference for Fe II EWs. This is probably related to a larger spread in velocity of the absorption lines in the H_2-bearing sample and therefore possibly larger metallicities.

The selected candidates would increase by a factor of 2 the number of known H_2 absorption systems at high redshift. It is important to note that we can confidently identify only saturated H_2 systems with high column densities, $\log N_{H_2} > 19$. To date there are only a few such systems detected at high redshift. The selected candidates will undoubtedly allow us to gather a large sample of HD detections. The relative abundance of HD/H_2 molecules which provides important clues on the chemistry and star formation history and also can be used to estimate the isotopic D/H ratio and consequently Ω_b – the density of baryonic matter in the Universe (Balashev et al. 2010; Ivanchik et al. 2010). In addition these systems are unique objects to search for CO molecule (Srianand et al. 2008). This molecule is suitable to estimate the physical conditions in interstellar clouds and the CMBR temperature at high redshift (Noterdaeme et al. 2010, 2011). We have selected four candidates with column densities $\log N_{H_2} > 20$. Such systems have never been observed at high redshifts towards QSO sightlines and would provide an exclusive opportunity to study translucent clouds in the ISM at high redshift.

ACKNOWLEDGEMENTS

REFERENCES

Abazajian K. N. et al., 2009, ApJS, 182, 543
Ahn C. P. et al., 2012, ApJS, 203, 21
Balashev S. A., Ivanchik A. V., Varshalovich D. A., 2010, Astron. Lett., 36, 761
Busca N. G. et al., 2013, A&A, 552, A96
Crighton N. H. M. et al., 2013, MNRAS, 433, 178
Cui J., Bechtold J., Ge J., Meyer D. M., 2005, ApJ, 633, 649
Dawson K. S. et al., 2013, AJ, 145, 10
Ellison S. L., Yan L., Hook I. M., Pettini M., Wall J. V., Shaver P., 2001, A&A, 379, 393
Fynbo J. P. U. et al., 2011, MNRAS, 413, 2481
Ge J., Bechtold J., 1997, ApJ, 477, L73
Guimarães R., Noterdaeme P., Petitjean P., Ledoux C., Srianand R., López S., Rahmani H., 2012, AJ, 143, 147
Ivanchik A., Petitjean P., Varshalovich D., Aracil B., Srianand R., Chand H., Ledoux C., Boissé P., 2005, A&A, 440, 45
Ivanchik A. V., Petitjean P., Balashev S. A., Srianand R., Varshalovich D. A., Ledoux C., Noterdaeme P., 2010, MNRAS, 404, 1583
Jorgenson R. A., Wolfe A. M., Prochaska J. X., Lu L., Howk J. C., Cooke J., Gawiser E., Gelino D. M., 2006, ApJ, 646, 730
Jorgenson R. A., Wolfe A. M., Prochaska J. X., Carswell R. F., 2009, ApJ, 704, 247
Jorgenson R. A., Wolfe A. M., Prochaska J. X., 2010, ApJ, 722, 460
Krogager J.-K., Fynbo J. P. U., Møller P., Ledoux C., Noterdaeme P., Christensen L., Milvang-Jensen B., Sparre M., 2012, MNRAS, 424, L1
Krühler T. et al., 2013, A&A, 557, A18
Krumholz M. R., 2012, ApJ, 759, 9
Ledoux C., Srianand R., Petitjean P., 2002, A&A, 392, 781
Ledoux C., Petitjean P., Srianand R., 2003, MNRAS, 346, 209
Ledoux C., Petitjean P., Srianand R., 2006, ApJ, 640, L25
Levshakov S. A., Varshalovich D. A., 1985, MNRAS, 212, 517
Malec A. L. et al., 2010, MNRAS, 403, 1541
Meiksin A. A., 2009, Rev. Modern Phys., 81, 1405
Noterdaeme P., Ledoux C., Petitjean P., Srianand R., 2008a, A&A, 481, 327
Noterdaeme P., Petitjean P., Ledoux C., Srianand R., Ivanchik A., 2008b, A&A, 491, 397
Noterdaeme P., Petitjean P., Ledoux C., Srianand R., 2009, A&A, 505, 1087
Noterdaeme P., Petitjean P., Ledoux C., López S., Srianand R., Vergani S. D., 2010, A&A, 523, A80
Noterdaeme P., Petitjean P., Srianand R., Ledoux C., López S., 2011, A&A, 526, L7
Noterdaeme P. et al., 2012, A&A, 547, L1
Pâris I. et al., 2011, A&A, 530, A50
Pâris I. et al., 2012, A&A, 548, A66
Petitjean P., Ledoux C., Noterdaeme P., Srianand R., 2006, A&A, 456, L9
Prochaska J. X., Wolfe A. M., 2009, ApJ, 696, 1543
Prochaska J. X. et al., 2009, ApJ, 691, L27
Quider A. M., Nestor D. B., Turnshek D. A., Rao S. M., Monier E. M., Weyant A. N., Busche J. R., 2011, AJ, 141, 137
Rachford B. L. et al., 2002, ApJ, 577, 221
Rahmani H. et al., 2013, MNRAS, 435, 861
Reimers D., Baade R., Quast R., Levshakov S. A., 2003, A&A, 410, 785
Schlafly E. F., Finkbeiner D. P., 2011, ApJ, 737, 103
Schlegel D. J., Finkbeiner D. P., Davis M., 1998, ApJ, 500, 525
Schlegel D. J. et al., 2007, Bull. Am. Astron. Soc., 39, 966
Schneider D. P. et al., 2010, AJ, 139, 2360
Smee S. A. et al., 2013, AJ, 146, 32
Songaila A. et al., 1994, Nature, 371, 43
Srianand R., Petitjean P., Ledoux C., 2000, Nature, 408, 931
Srianand R., Petitjean P., Ledoux C., Ferland G., Shaw G., 2005, MNRAS, 362, 549
Srianand R., Noterdaeme P., Ledoux C., Petitjean P., 2008, A&A, 482, L39
Thompson R. I., 1975, Astrophys. Lett., 16, 3
Vanden Berk D. E. et al., 2001, AJ, 122, 549
Varshalovich D. A., Ivanchik A. V., Petitjean P., Srianand R., Ledoux C., 2001, Astron. Lett., 27, 683
Wendt M., Molaro P., 2012, A&A, 541, A69
York D. G. et al., 2000, AJ, 120, 1579
Zhu G., Ménard B., 2013, ApJ, 770, 130

This paper has been typeset from a TEX/LATEX file prepared by the author.